

## Rotational Fluctuations of Water Confined to Layered Oxide Materials: Nonmonotonous Temperature Dependence of Relaxation Times

Ligia Frunza,<sup>\*,†</sup> Andreas Schönhals,<sup>‡</sup> Stefan Frunza,<sup>†</sup> Vasile I. Parvulescu,<sup>§</sup> Bogdan Cojocaru,<sup>§</sup> Daniel Carriazo,<sup>||</sup> Cristina Martín,<sup>||</sup> and Vicente Rives<sup>||</sup>

National Institute of Materials Physics, R-077125 Magurele, Romania, Federal Institute of Materials Research and Testing, D-12205 Berlin, Germany, Department of Chemical Technology and Catalysis, Faculty of Chemistry, University of Bucharest, R-030016 Bucharest, Romania, and Departamento de Química Inorgánica, Universidad de Salamanca, E-037008 Salamanca, Spain

Received: March 2, 2007; In Final Form: April 20, 2007

The rotational molecular dynamics of water confined to layered oxide materials with brucite structure was studied by dielectric spectroscopy in the frequency range from  $10^{-2}$  to  $10^7$  Hz and in a broad temperature interval. The layered double hydroxide samples show one relaxation process, which was assigned to fluctuations of water molecules forming a layer, strongly adsorbed to the oxide surface. The temperature dependence of the relaxation rates has an unusual saddlelike shape characterized by a maximum. The model of Ryabov et al. (*J. Phys. Chem. B* **2001**, *105*, 1845) recently applied to describe the dynamics of water molecules in porous glasses is employed also for the layered materials. This model assumes two competing effects: rotational fluctuations of water molecules that take place simultaneously with defect formation, allowing the creation of free volume necessary for reorientation. The activation energy of rotational fluctuations, the energy of defect formation, a pre-exponential factor, and the defect concentration are obtained as main parameters from a fit of this model to the data. The values of these parameters were compared with those found for water confined to nanoporous molecular sieves, porous glasses, or bulk ice. Several correlations were discussed in detail, such as the lower the value of the energy of defect formation, the higher the number of defects. The pre-exponential factor increases with increasing activation energy, as an expression of the compensation law, and indicates the cooperative nature of the motional process. The involvement of the surface OH groups and of the oxygen atoms of the interlayer anions in the formation of hydrogen bonds was further discussed. For the birnessite sample, the relaxation processes are probably overlaid by a dominating conductivity contribution, which is analyzed in its frequency and temperature dependence. It is found that the conductivity of birnessite obeys the characteristics of semiconducting disordered materials. Especially the Barton/Nakajima/Namikawa relationship is fulfilled. Analyzing the temperature dependence of the direct current (dc) conductivity  $\sigma_0$  in detail gives some hint that  $\sigma_0(T)$  has also an unusual saddlelike form.

### Introduction

Water plays a major role in a wide range of systems, such as various geological, biological, and technological materials. Most of these systems have in common that the water is dispersed in small nanosized pores or cavities. Then the properties of water are influenced by the restricted space as well as by the interactions with its environment.

Recently, the dynamics of water molecules in the pores of SBA-type molecular sieves was investigated by broadband dielectric spectroscopy in a wide temperature range.<sup>1</sup> Two relaxation processes have been observed, which are separated by 7 orders of magnitude in the frequency scale. Both of these processes were assigned to rotational fluctuations of water molecules: the process at lower frequencies was assigned to molecules forming a surface layer close to the pore wall,

whereas the relaxation process at higher frequencies above 1 MHz was assigned to water molecules forming a second layer located close to the center of the pores. In the former case the molecules strongly interact (by hydrogen bonds) with the surface OH groups. The relaxation rate of this low-frequency process has an unusual saddlelike temperature dependence characterized by a maximum. To describe this temperature dependence, the Ryabov model<sup>2</sup> was used, which assumes a counterbalance of two competing processes: orientational fluctuations of the water molecules and defect formation in the vicinity of a fluctuating water molecule. Defects might be formed because the rotational fluctuation of a molecule always involves the breaking of hydrogen bonds to reach other sites. For water molecules confined to other molecular sieves, the saddlelike temperature dependence occurs for the processes at higher frequencies as well.<sup>3</sup> Moreover, a similar temperature dependence was found for a variety of other confining hosts, including nanoporous glasses.<sup>2b</sup> Thus, this nonmonotonous behavior was found to be a rather general characteristic for water confined to nanopores.

Therefore, it is important to study the dynamics of water molecules in a broad frequency and wide temperature range

\* Corresponding author: tel +40 21 3690185; fax +40 21 3690177; e-mail lfrunza@infim.ro.

<sup>†</sup> National Institute of Materials Physics.

<sup>‡</sup> Federal Institute of Materials Research and Testing.

<sup>§</sup> University of Bucharest.

<sup>||</sup> Universidad de Salamanca.

**TABLE 1: Composition and Specific Surface Area of the Samples**

sample	M, <sup>a</sup> wt %	Al, wt %	Mo, wt %	Mn, wt %	M/Al <sup>b</sup>	formula	S <sub>BET</sub> , <sup>c</sup> m <sup>2</sup> g <sup>-1</sup>
ZnAlMo	24.1	5.3	24.1		1.9	[Zn <sub>0.66</sub> Al <sub>0.34</sub> (OH) <sub>2</sub> ](Mo <sub>7</sub> O <sub>24</sub> ) <sub>0.06</sub> <sup>d</sup>	43
NiAlMo	24.5	5.3	22.2		2.1	[Ni <sub>0.68</sub> Al <sub>0.32</sub> (OH) <sub>2</sub> ](Mo <sub>7</sub> O <sub>24</sub> ) <sub>0.05</sub> <sup>d</sup>	34
NaBIR	7.0	0	50.9	50.9		Na <sub>0.33</sub> MnO <sub>2</sub> ·0.91H <sub>2</sub> O	29

<sup>a</sup> For LDH materials, M is the divalent metallic cation (zinc or nickel) in the framework; for birnessite, M is the cation in the interlayer, here monovalent sodium ion. <sup>b</sup> Molar ratio. <sup>c</sup> Determined by nitrogen absorption via the single-point method.<sup>12</sup> <sup>d</sup> In the dehydrated form.

also for other confining materials having a different structure than nanoporous glasses, molecular sieves with cylindrical pores or faujasite-like cavities. So here layered oxide materials are considered, which have structural disorder related to chemical, crystallographic, and physical heterogeneities. These heterogeneities can be regarded also as defects, which might interfere with the discussed interaction of water molecules by hydrogen bonds with surface OH groups. It is expected that the temperature dependence of the relaxation rates is also changed in comparison with conventional laws like the Arrhenius or the Vogel/Fulcher/Tammann (VFT) dependence.

Another reason to investigate the molecular mobility of water in such materials is related to their applicability in catalytic reactions: These reactions might take place in aqueous solutions or water molecules that are obtained among the reaction products. In addition, the molecular structure and the molecular mobility of the first few interfacial adsorbed layers—which play a critical role in many processes<sup>4,5</sup>—become important under confinement conditions (confinement-induced disorder<sup>6</sup>). Besides that, experimental studies probing the interlayer, the surface regions, and even the detailed structure of the sheets are difficult and scarcely discussed in the literature.

Here we report on the dynamics of water molecules in layered oxide materials that differ by the sign and the number of charges of the layers. The layers are either positively charged, as in the case of layered double hydroxides (LDHs), or negatively charged, as for birnessite-type materials. Because the systems have to be electroneutral, in the interlayer space these materials contain either anions (LDHs) or cations (birnessite sample). Water molecules are also located in the interlayer space.

We expected changes in the dielectric properties of layered oxide materials with the composition due to the subtle balance of different forces including Coulomb repulsion, steric hindrance, and hydrophobic/hydrophilic interactions. Significant differences between the considered samples, which were related to their structure, are found.

## Experimental Section

**Layered Oxide Materials.** As is known, the structure of the layered double hydroxides (and of hydroxalicates as well) is similar to that of brucite [Mg(OH)<sub>2</sub>], where each magnesium cation is octahedrally surrounded by hydroxyl groups. An isomorphous substitution of Mg<sup>2+</sup> by trivalent or other divalent cations occurs in the LDHs. When the Mg<sup>2+</sup> ions are replaced by a trivalent ion, a positive charge is generated in the brucite sheet, which is otherwise electroneutral. The positive charge is compensated by anions in the interlayer. In these interlayer galleries, water molecules also exist. Therefore, the LDH compounds are generally described<sup>7,8</sup> by the formula [M<sub>1-x</sub><sup>2+</sup>M<sub>x</sub><sup>3+</sup>(OH)<sub>2</sub>]<sup>+</sup>(A<sup>-</sup>)<sub>x/z</sub>·mH<sub>2</sub>O, where M<sup>2+</sup> and M<sup>3+</sup> are the metal cations and A<sup>-</sup> represents the anions to balance the positive charge of the layer. In our case M<sup>2+</sup> = Zn<sup>2+</sup> or Ni<sup>2+</sup>; M<sup>3+</sup> = Al<sup>3+</sup>, and A<sup>-</sup> = heptamolybdate anions (Mo<sub>7</sub>O<sub>24</sub><sup>6-</sup>). The different LDH-heptamolybdate samples were prepared following the exchange method with LDH-terephthalate as a precursor.<sup>9,10</sup> Following their composition (Table 1), the sample codes are ZnAlMo and NiAlMo.

LDH materials were characterized by elemental analysis, powder X-ray diffraction, Fourier transform infrared spectroscopy (FTIR) (KBr technique), and nitrogen adsorption.<sup>9,10</sup>

Birnessite is a manganese dioxide (MnO<sub>2</sub>) having a brucite-like structure as well. It consists of layers of edge-sharing MnO<sub>6</sub> octahedra; their negative charge arises from vacancies of tetravalent manganese ions and from their substitution with other ions having a lower valence state like Mn<sup>2+</sup> and Mn<sup>3+</sup>.<sup>11</sup> This charge is compensated by protons or interlayer cations: In our case, there are sodium cations and water molecules in the interlayer. The sample (further labeled NaBIR) was prepared by a sol-gel method<sup>12-14</sup> with a glucose/NaMnO<sub>4</sub> molar ratio of 1. It was characterized as described above for LDH samples. Its composition is given in Table 1 as well.

**Dielectric Measurements.** Self-supported pellets were pressed for the dielectric investigations just before the measurements and then handled in desiccators. This preparation has been described in detail elsewhere.<sup>1</sup> In brief, the powder of layered material was gently pressed into self-supported pellets. To remove impurities, the samples were treated under vacuum (10<sup>-2</sup> Torr) at ca. 500 K for 2 h. After that, the samples were cooled down to room temperature under vacuum and then contacted for more than 24 h in a water vapor atmosphere with a relative humidity as provided by a saturated Ca(NO<sub>3</sub>)<sub>2</sub> solution in a closed vessel.<sup>15</sup> The water content of the samples was determined by thermogravimetric (TG) analysis (see below). The pellets were placed in a capacitor arrangement with parallel plate geometry. The measurements were not conducted in a closed cell but in a nitrogen stream, ensuring not only thermal equilibration but also protection of the sample from the surrounding atmosphere.

The complex dielectric function  $\epsilon^*(f) = \epsilon'(f) - i\epsilon''(f)$  (where  $f$  = frequency,  $\epsilon'$  = real part, and  $\epsilon''$  = loss part) was measured in the frequency range from 10<sup>-2</sup> to 10<sup>7</sup> Hz by a Novocontrol high-resolution Alpha analyzer. The dielectric measurements were carried out under isothermal conditions; the temperature was controlled by a Novocontrol Quatro Cryosystem with a stability better than 0.1 K. The temperature was increased stepwise from 220 to 428 K in steps of 3 K.

The model function of Havriliak-Negami (HN function) was employed to analyze and to separate the different relaxation processes (details can be found in refs 16 and 17a). The HN function reads

$$\epsilon^*(f) - \epsilon_\infty = \frac{\Delta\epsilon}{[1 + (if/f_0)^\beta]^\gamma} \quad (1)$$

where  $f_0$  is a characteristic frequency related to the frequency of maximal loss  $f_p$  (relaxation rate) of the relaxation process under consideration, and  $\epsilon_\infty$  describes the value of the real part  $\epsilon'$  for  $f \gg f_0$ .  $\beta$  and  $\gamma$  are fractional form parameters ( $0 < \beta \leq 1$  and  $0 < \beta\gamma \leq 1$ ) characterizing the shape of the relaxation time spectra.  $\Delta\epsilon$  denotes the dielectric strength, which is proportional to the mean squared effective dipole moment and to the number of the fluctuating dipoles per unit volume. Conduction effects were treated in the usual way by adding a

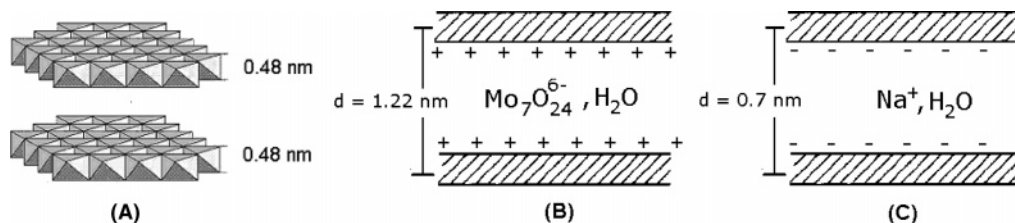


**Figure 1.** Schematic representation of the layered structure: (A) brucite-like sheets; (B) LDH and (C) birnessite samples.

conductivity contribution  $\sigma_0/\epsilon_0(2\pi f)^x$  to the dielectric loss.  $\sigma_0$  is related to the dc conductivity of the sample, and  $\epsilon_0$  is the dielectric permittivity of vacuum. The parameter  $x$  ( $0 < x \leq 1$ ) describes for  $x < 1$  non-Ohmic effects in the conductivity. For details see ref 17a. As the real and the imaginary part of the dielectric function are related to each other by the Kramers–Kronig relationships, meaning that both quantities carry the same information, only the dielectric loss is considered. The results are discussed by use of the temperature dependence of the relaxation rate  $f_p$  and of the dielectric strength  $\Delta\epsilon$ .

Alternatively to the complex dielectric function, the complex electric conductivity  $\sigma^*$  is used to describe the dielectric behavior. Its relationship to the complex dielectric function is given by

$$\sigma^*(f) = i2\pi f\epsilon_0\epsilon^*(f) \quad (2)$$

with the real part<sup>17b</sup>

$$\sigma'(f) = 2\pi f\epsilon_0\epsilon''(f) \quad (3)$$

The water loading degree  $c_w$  was estimated by thermogravimetric measurements as already described for different other composites.<sup>18</sup> These measurements were performed by a Setaram TG-DTA 92 apparatus, under a dry, oil-free air atmosphere, using a part of the sample prepared for dielectric measurements. Taking the density of confined water as  $\rho_w^{\text{conf}} \approx 1 \text{ g cm}^{-3}$ , the layer thickness  $h_w^{\text{conf}}$  of the confined water was roughly estimated as  $h_w^{\text{conf}} = (c_w/\rho_w^{\text{conf}})S_{\text{BET}}$ .

## Results and Discussion

**Structure of the Layered Oxide Materials.** A sketch of the sheetlike structure of the materials is given in Figure 1A: Each layer is 0.48 nm thick<sup>18</sup> and contains edge-sharing octahedra. The interlayer distance is a function of the hydrating degree and of the size of the ions intercalated in the interlayer. The layer composition is as follows:  $[\text{M}_{1-x}^{2+}\text{M}_x^{3+}(\text{OH})_2]^{x+}$  for LDH sample and  $[\text{Mn}_{1-x-y-u}^{4+}\text{Mn}_x^{2+}\text{Mn}_y^{3+}u\text{O}_2]^{(2x+y+4u)-}$  for birnessite one ( $\square^{4+}$  is a vacancy of a cation with the charge 4+). In Figure 1B,C, the interlayer composition is given for both LDH- and birnessite-type materials. The interlayer voids may have prismatic or octahedral structures depending whether the opposing ions of adjacent layers like hydroxyl groups in LDH samples or oxygen ions in birnessite lie vertically above one another or offset in close-packed positions.

Another important feature is the hydrogen bonding of water molecules with surface components or with interlayer particles. In fact, it was shown that hydrogen bonding is important for maintaining the stability of the expanded interlayer region.<sup>20</sup> Dehydration is complex leading to a gradual, concerted layer collapse as temperature is raised and water is lost. Compared to dehydrating, hydrating is a slow process occurring over a few days.<sup>20</sup>

The X-ray diffraction (XRD) diagrams of the investigated LDH samples show the characteristic features of layered

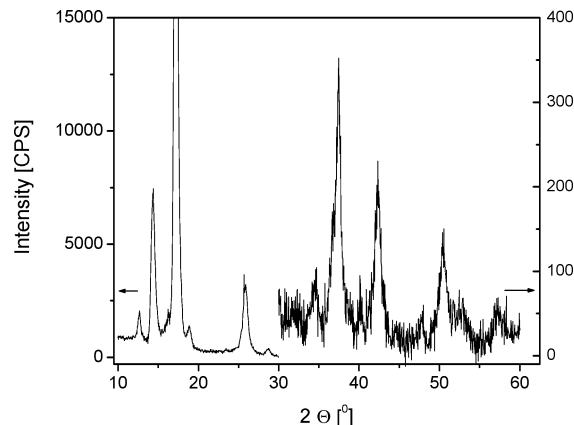


**Figure 2.** X-ray diffraction pattern for NaBIR. Between 30° and 60°, the ordinate scale is enlarged due to the low intensity of the reflections.

compounds.<sup>10</sup> It is beyond the scope of this paper to discuss in detail these diagrams. Thus we will highlight here only some relevant details in brief. Indexing of the powder patterns is based on the hexagonal unit cells, although the structures described are mostly rhombohedral. The use of hexagonal indices simplifies the comparison to related materials.

Some aspects of the order/disorder features of these samples can be deduced from these XRD patterns. Among the LDH samples, the sharpest XRD peaks are observed for the sample ZnAlMo.<sup>12</sup> They are symmetric, suggesting an ordered stacking of the layers.

An interlayer space distance of 0.72 nm is obtained from XRD data for the LDH samples when the thickness of the brucite-like layer is subtracted from the basal spacing (1.2 nm). This value roughly coincides with that calculated for the size of the heptamolybdate ion with its  $C_2$  axis perpendicular to the layers, in agreement with similar systems with heptamolybdate intercalated in Mg–Al and Zn–Al LDHs.<sup>21</sup> As is well established,<sup>22</sup> two orientations of heptamolybdate anions in the interlayer are possible: one orientation leads to a pattern with two basal reflections at 0.60 and 0.40 nm, which can be indexed as (006) and (009). The other orientation leads to a pattern with two basal reflections at 0.68 and 0.40 nm with the same indexing. Since a clear assignment of these peaks in the XRD patterns is difficult, the preferential orientation of heptamolybdate anions in the investigated LDH samples was performed on the basis of the relative intensity of the main peaks: the former orientation seems to be preferred. Evidence for the intercalation of the heptamolybdate anions is additionally provided by Raman<sup>9</sup> and IR spectroscopy as well.<sup>10</sup>

The birnessite sample is also a highly ordered brucite-like material, as can be seen from its XRD pattern (Figure 2). This pattern can be indexed by use of a three-layer rhombohedral unit cell as already described.<sup>23,24</sup> Going from the low- to the high-angle values, the powder pattern contains reflections with  $d(00l)$  values corresponding to a minimum periodicity of 0.7 nm along the  $c$ -axis followed by families of  $hkl$  reflections. Considering the intensities of the latter ones, one can appreciate

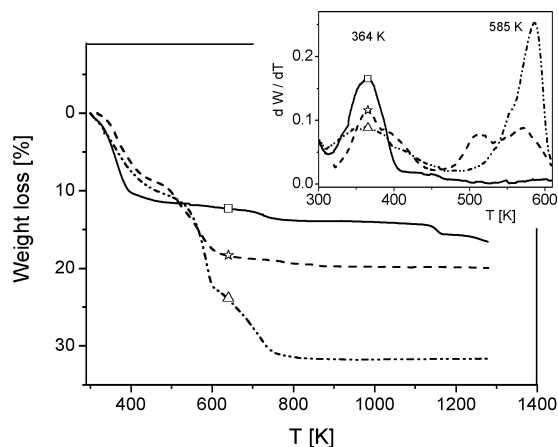


**Figure 3.** TG curves for the investigated samples: (□, —) NaBIR; (☆, ---) NiAlMo; (△, -·-·-) ZnAlMo. (Inset) Corresponding derivatives on an enlarged temperature scale.

**TABLE 2: Weight Loss and Content of the Confined Water**

sample	(W1 + W2), <sup>a</sup> %	(W4 + W5), <sup>b</sup> %	$h_w^{\text{conf}}$ , nm
ZnAlMo	9.1	10.9	2.3
NiAlMo	10.1	21.9	3.2
NaBIR	11.3	2.7	4.3

<sup>a</sup> Sum of first and second water loss (up to 473 K). <sup>b</sup> Sum of last two weight losses (between 473 and 973 K).

that the investigated birnessite corresponds to a mixture of polytypes,<sup>23,24</sup> those leading to prismatic structures (to accommodate interlayer species) of the interlayer being predominantly oriented perpendicular with regard to those leading to octahedral voids.

**Thermogravimetric Analysis.** Thermogravimetric and differential thermal analyses of all samples were carried out in synthetic air. Representative TG curves together with the corresponding DTG curves are shown in Figure 3. Thermogravimetric parameters for the samples studied are summarized in Table 2. The LDH samples undergo a progressive weight loss in four steps when the temperature increases. There are ill-defined inflection points that can hardly be distinguished in the TG curves. However, the temperature interval for each step was clarified by discussing the associated DTG and DTA curves too. The first two weight-loss steps covering the interval till 450 K are due to the removal of weakly bonded water molecules, physisorbed on the surface or positioned in the interlayer spaces.<sup>25,26</sup> At higher temperatures the chemical process of dehydroxylation of the brucite-like layers starts, where the water molecules formed by the reaction further desorb. Finally a third endothermic effect, extended up to ca. 590 K, is observed. These three processes lead to the collapse of the layered structure. A fourth step or possibly even more steps has/have also chemical origins, which are related to the transformation and/or removal of the interlayer anion.<sup>24</sup> It is noteworthy that the dielectric measurements are performed in the low-temperature range where only physical desorption processes take place, and so the structure of the materials is maintained.

In the case of birnessite sample, there are also four distinct processes of weight losses (Figure 3). The two low-temperature losses are commonly assigned to the removal of adsorbed and interlayer water. The process occurring between 523 and 673 K likely corresponds to the loss of oxygen atoms from the octahedral layer framework in relation to the partial reduction of  $\text{Mn}^{4+}$  to  $\text{Mn}^{3+}$ .<sup>24</sup> This leads also to distortions in the structure because  $\text{Mn}^{3+}$  cations are known indeed to be affected by the Jahn–Teller effect that lowers the symmetry of the 3d electron

orbitals and distorts the octahedra. Besides, this weight loss likely results from the migration of vacant layer octahedra and induces the formation of vacancy-free layers. Therefore, the weight loss observed at temperatures higher than 673 K may be considered as evidence for the presence of vacant layer sites in the sample. The weight loss in the same temperature range can be alternatively related to some dehydroxylation process involving OH groups initially bonded to pre-existing  $\text{Mn}^{3+}$  cations.

The water content (Table 2) was calculated considering the weight loss up to a temperature of 470 K.

Finally, the strong endothermic peak at ca. 1100 K most likely is related to the birnessite melting, as observed in the case of K-birnessite.<sup>24</sup>

More information about the structure of the layered materials related to water comes from modeling the hydration of hydroxalicates.<sup>27</sup> It was shown that the Al polyhedra in the hydroxide layers are quite regular; instead, the Mg polyhedra are distorted ones. In addition, most of the Mg cations have either a water molecule or an interlayer anion coordinated, thus forming a 7-coordinate site. The displacement of Mg atoms from the middle of the hydroxide layers results in the formation of a much less regular network of hydrogen atoms. Beside the Mg cations there is a second kind of a positively charged attractive site on the hydroxide layer, formed by the protons of the hydroxyl groups, which are thus able to form hydrogen bonds with the interlayer anions. These strongly hydrogen-bonded anions become in turn virtually immobile even at high temperatures.

**Dielectric Spectroscopy.** The dielectric properties of the layered materials are quite different with regard to their conductivity. Particularly the conductivity of NaBIR is orders of magnitude higher than that of the LDHs. This is probably due to the different mobility and charges of the ions in the interlayer of the different materials. For this reason each material is first discussed separately. A comparison is given at the end.

(a) *NiAlMo.* A 3D plot of the dielectric loss as function of frequency and temperature is given in Figure 4A for the sample NiAlMo. In the investigated frequency range, several dielectric phenomena can be observed, like a Maxwell–Wagner polarization effect (due to the blocking of charge carriers at the grain boundaries) and a dc conduction at low frequencies, as was the case in related porous materials.<sup>3,28</sup> In addition to that, one dielectric relaxation process, indicated by a peak in the dielectric loss, is observed. For experimental reasons the materials could not be investigated in the fully dehydrated state. So it is argued that this relaxation process has to be assigned to the constrained rotational dynamics of water molecules confined in the interlayer galleries of NiAlMo for the following reasons: It is well-known that in the experimental frequency and temperature window no relaxation process due to silica (a material related to LDHs) itself or to bulk liquid water molecules is expected.<sup>29,30</sup> Therefore, a similar behavior is supposed for NiAlMo. Moreover, it was already shown for AIMCM-41,<sup>27</sup> porous glass,<sup>31</sup> and Anopore membranes<sup>32</sup> that the contribution of the pore wall material (motions of the silica/alumina tetrahedra as building groups) to the dielectric loss is negligibly small (3 orders of magnitude lower) compared to that observed for the (liquid) loaded samples. In addition, the exchanged cations generally contribute mostly to the dc conductivity.<sup>33</sup> Moreover, after the sample is heated up, no relaxation process can be observed by the dielectric measurements carried out during the cooling. This is a supplementary argument that the observed process is related to rotational fluctuations of water molecules. Consequently, this

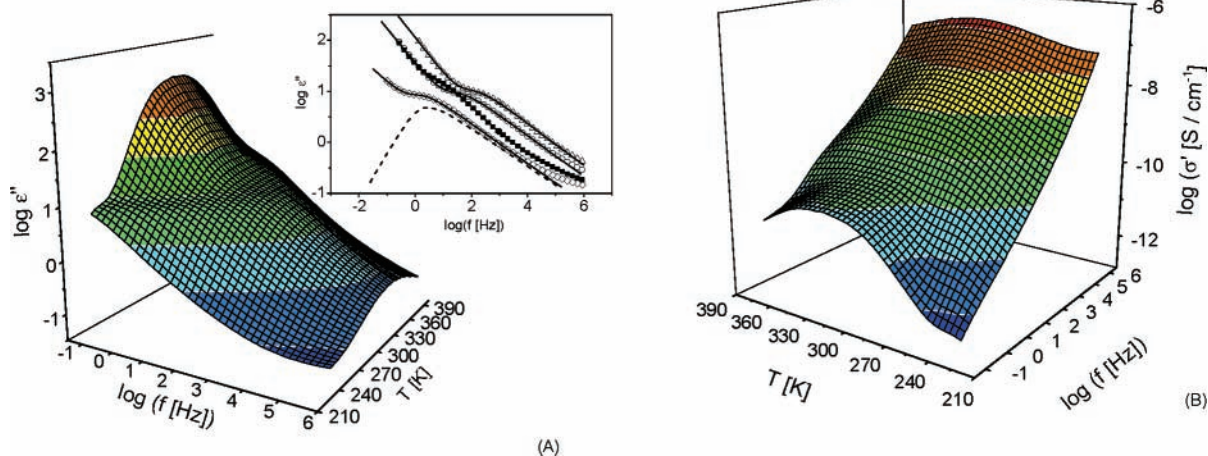


**Figure 4.** (A) Dielectric loss of NiAlMo vs frequency and temperature in a 3D representation. (Inset) Dielectric loss vs frequency for different temperatures: ( $\diamond$ ) 253.2, ( $\circ$ ) 283.2, ( $\triangle$ ) 313.2, and ( $\blacksquare$ ) 373.2 K. Lines are fits of the HN equation to the data. (---) Relaxational contribution for  $T = 253.2$  K, having the HN parameters  $\beta = 0.96$ ,  $\gamma = 0.46$ ,  $\log(\sigma_0/\epsilon_0) = 1.1$ , and  $x = 0.38$ . (B) Real part of the complex conductivity of NiAlMo vs frequency and temperature in a 3D representation.

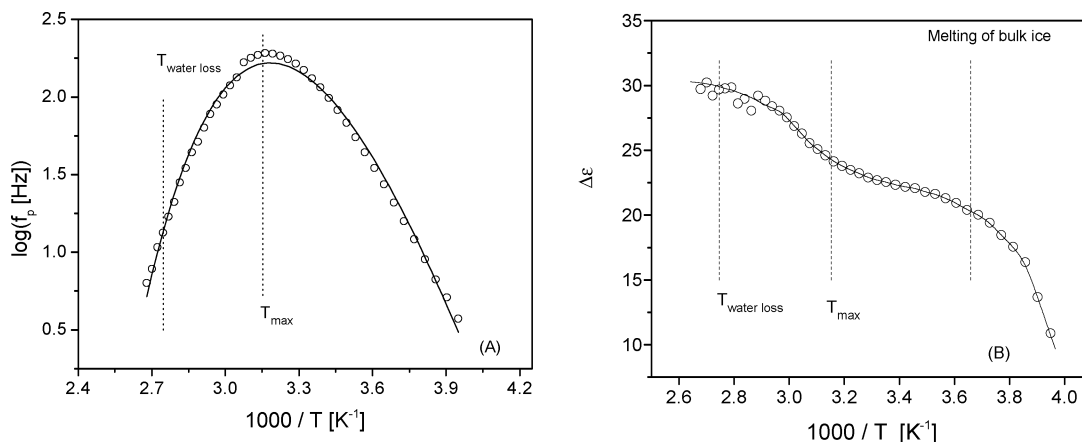


**Figure 5.** (A) Relaxation rate vs reciprocal temperature for NiAlMo. The line is a fit of eq 5 to the data. (B)  $\Delta\epsilon$  vs reciprocal temperature for NiAlMo. The line is a guide for the eyes.

process is assigned to the rotational dynamics of water molecules in the interlayer galleries of the LDH material and it is discussed in the following in detail.

The observed long relaxation times in comparison to bulk water lead to the conclusion that the involved water molecules are constrained and are in close contact with the confining LDH surface. In related systems, such constrained water molecules in close contact to confining surfaces (layers) were confirmed, for example, for water in MCM-41 molecular sieves, by line-shape analysis of  $^2\text{H}$  double-quantum-filtered NMR and  $T_1$  measurements.<sup>34</sup>

The relaxation process has an unusual behavior with regard to the temperature dependence of its mean relaxation rate. With increasing temperature, the maximum of the dielectric loss shifts to higher frequencies, as expected (see inset in Figure 4A). The extrapolation of this dependence at low temperatures to room temperature gives a relaxation rate of 165 Hz, which is essentially lower than the value of free bulk water,<sup>35</sup> which is about 20 GHz. After a certain temperature is reached, the maximum position of the dielectric loss moves down to lower frequencies with further increase of temperature (see inset in Figure 4A).

Because the dielectric loss is related to the conductivity (see eqs 2 and 3), the temperature dependence of conductivity follows that of the dielectric loss (Figure 4B): At low temperatures the

conductivity increases up to a maximum value, and then it decreases with further increase of temperature.

The temperature dependence of the relaxation rate is represented in Figure 5A. As already seen in the raw data,  $f_p$  increases with temperature up to a maximum value observed at  $T_{\text{max}} = 317$  K. Above  $T_{\text{max}}$ ,  $f_p$  decreases with further increase of temperature. This unusual temperature dependence of the relaxation rate should be not predominantly related to a loss of water. First, it is noted that  $T_{\text{max}}$  is essentially lower than the temperature found for the maximal loss of water. Second, the dielectric strength  $\Delta\epsilon$  increases with temperature in the whole temperature range investigated (see Figure 5B). The Debye theory of dielectric relaxation generalized by Kirkwood and Fröhlich<sup>17c</sup> predicts for the temperature dependence of the dielectric relaxation strength

$$\Delta\epsilon = \frac{1}{3\epsilon_0} g \frac{\mu^2 N}{k_B T V} \quad (4)$$

where  $\mu$  is the mean dipole moment of the process under consideration and  $N/V$  is the number density of dipoles involved.  $g$  is the so-called Kirkwood/Fröhlich correlation factor, which describes static correlation between the dipoles. Because  $\Delta\epsilon$  is proportional to the number density of fluctuating dipoles, a substantial loss of water should lead to a decrease of the dielectric strength instead of the observed increase because the number density of water molecules decreases. There seem to

**TABLE 3: Parameters Characterizing Temperature Dependencies of the Relaxation Rates Obtained by Fitting Eq 5 to the Data<sup>a</sup>**

sample	$E_a$ , kJ/mol	$E_d$ , kJ/mol	$-\log(\tau[\text{s}])$	$1/C$	max no. of defects	ref
NiAlMo	97.7	14.2	20.6	$6.3 \times 10^{-4}$	$10^{20}$	this work
ZnAlMo	75.4	10.5	17.3	$3.48 \times 10^{-2}$	$1.5 \times 10^{20}$	this work
AlSBA-15	50.8	25.4	13.0	$5.8 \times 10^{-6}$	$10^{19}$	1
NMSF	48.1	31.3	12.8	$7.7 \times 10^{-7}$	$10^{18}$	1
porous glass	55–42	39–30	13.5–12.1	$9 \times 10^{-7}$ – $2 \times 10^{-5}$	$10^{16}$ – $10^{17}$	2
NaY	19.6	22.6	17.8	$4 \times 10^{-4}$	$2.4 \times 10^{20}$	3
vermiculite <sup>b</sup>	40.4		~14			37

<sup>a</sup> Temperature dependence of the relaxation times was determined only between 125 and 225 K and obeys an Arrhenius law in this temperature range. <sup>b</sup> Layered clay (aluminum phyllosilicate).

be changes in the temperature dependence of  $\Delta\epsilon$  around the melting point of bulk water and at  $T_{\max}$ . At high temperatures a plateau level is observed. These changes might be related to different structure of the confined water, which can be described by different  $g$ -values including its temperature dependence. This needs further investigation.

Neither the Arrhenius nor the Vogel/Fulcher/Tammann equation<sup>36</sup> can be used to describe the whole temperature dependence of  $f_p$ . An adequate description of this unusual nonmonotonous temperature dependence of the relaxation rate is given by the model developed by Ryabov et al.<sup>2</sup> It was recently applied to describe the relaxation of water in nanoporous glasses,<sup>2a</sup> in the sodalite cages of faujasite,<sup>3</sup> and for water confined to other systems.<sup>2b</sup> The model assumes that the saddlelike temperature dependence of the relaxation rate must be due to the counterbalance of two competing processes. First, for rotational fluctuations the water molecules have to overcome energy barriers leading to Arrhenius-like temperature dependence  $\sim \exp[E_a/(k_B T)]$ .  $E_a$  is the height of the potential barriers between substates and  $k_B$  is the Boltzmann constant. Second, in the vicinity of a selected water molecule, a certain amount of free volume should be available for its reorientation, which can be provided by a defect. For the temperature dependence of the defect concentration  $\sim C \exp[-E_d/(k_B T)]$  was supposed, where  $E_d$  is the energy of the defect formation and  $C$  is the inverse maximum of the defect concentration.  $C$  determines mainly the value of the relaxation rate at the maximum temperature. For the relaxation time (or rate) the following expression

$$\frac{1}{2\pi f_p} = \tau = \tau_\infty \exp\left[\frac{E_a}{k_B T} + C \exp\left(-\frac{E_d}{k_B T}\right)\right] \quad (5)$$

was derived.<sup>2</sup> Equation 5 was fitted to the temperature dependence of the relaxation rate of NiAlMo. The estimated parameters are given in Table 3 along with values for related systems.

(b) *ZnAlMo*. The relaxation behavior of ZnAlMo is similar than that of NiAlMo but less pronounced. Figure 6 represents the dielectric loss as function of frequency for the three layered materials at room temperature for a direct comparison. One relaxation process is observed as indicated by a peak in the dielectric loss.

The relaxation rates of ZnAlMo are plotted versus reciprocal temperature in Figure 7A, while the variation of the dielectric strength with  $1/T$  is given in Figure 7B. As for NiAlMo, the temperature dependence of the relaxation rates is saddlelike with a maximum temperature  $T_{\max} = 325$  K. The parameters of the fit with the Ryabov model are given in Table 3.

Also, the dielectric strength of ZnAlMo increases with increasing temperature (Figure 7B). It is worth noting that, as for NiAlMo, a slight change in the temperature dependence of  $\Delta\epsilon$  is also observed for ZnAlMo at the melting point of bulk

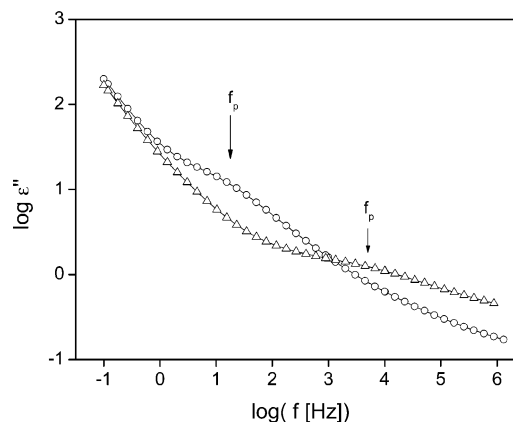


**Figure 6.** Comparison of the dielectric losses of ZnAlMo (○) and NiAlMo (△) at 373 K. Lines are guides for the eyes. Arrows indicate the relaxation process.

ice. Around  $T_{\max}$  a plateau-like structure is observed, but for higher temperatures  $\Delta\epsilon$  increases further with temperature.

The maximum number of defects per mole of adsorbed water is estimated in the range from  $10^{20}$  to  $10^{21}$  for both LDH materials. These values are higher than those found for water confined to nanoporous materials such as glasses, AlSBA-15, or nanoporous molecular sieves with foam-like structure. They are even higher compared to that found in bulk ice (cited in ref 2). This might suggest that more defects can be formed in water adsorbed in the layered oxide materials than in nanoporous molecular sieves/glasses or in bulk ice. So in the layered oxide materials there are more possibilities for defect formation than in the other confining systems. There is a correlation between the value of the energy of defect formation  $E_d$  and the number of defects of the adsorbed water structure (see Figure 8). For samples with a lower  $E_d$  value, the number of defects is higher. This seems to be reasonable, because the lower the energy of defect formation, the more easily defects can be formed.

The values found for the activation energy of the rotational fluctuations of the water molecules in the LDH materials are higher than those found for related materials (see Table 3). This might be due to confinement effects of the interlayer galleries on the structure of embedded water, which changes the internal rotational barriers. Also the corresponding values of  $\tau_\infty$  are higher than those for water in porous glass and nanoporous molecular sieves. In Figure 9 it is shown that  $-\log \tau_\infty$  increases with the activation energy  $E_a$ . Moreover, the data obtained for the LDH materials collapse into one line together with that obtained for porous glasses and molecular sieves. This is an expression of the well-known compensation law indicating the cooperative nature of the underlying motional processes.<sup>37</sup>

The values of the activation energy  $E_a$  (Table 3) are slightly smaller than those found for proton hopping between neighboring Al sites in molecular sieves ( $89$ – $126$  kJ mol<sup>-1</sup>).<sup>33</sup> So these

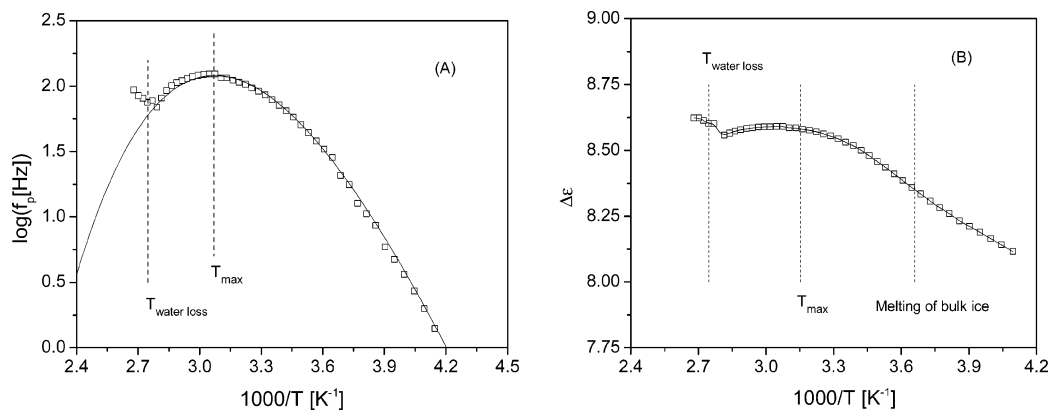


**Figure 7.** (A) Relaxation rates vs reciprocal temperature for ZnAlMo. The line is a fit of eq 5 to the data. (B) Dielectric strength vs reciprocal temperature for the same sample. The line is a guide for the eyes.

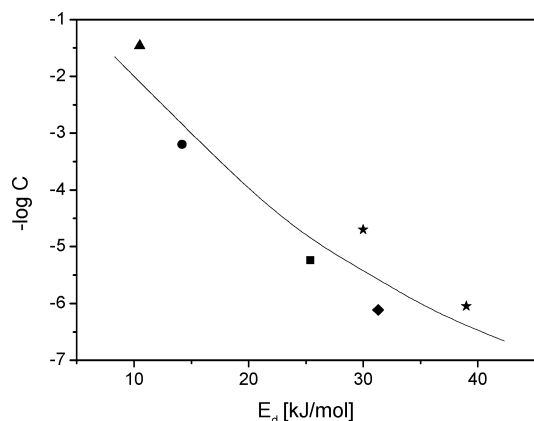


**Figure 8.** Inverse of maximum defect concentration vs energy of defect formation: (●) NiAlMo; (▲) ZnAlMo, (■) AISBA-15,<sup>1</sup> (◆) NMSF,<sup>1</sup> and (★) nanoporous glasses.<sup>2b</sup> The line is a guide for the eyes.

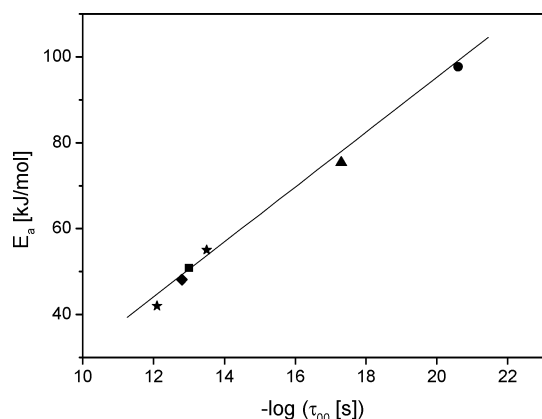


**Figure 9.** Correlation of  $\log \tau_{\infty}$  and  $E_a$  in the compensation plot: (●) NiAlMo; (▲) ZnAlMo, (■) AISBA-15,<sup>1</sup> (◆) NMSF,<sup>1</sup> and (★) nanoporous glasses.<sup>2b</sup> The line is a linear regression through all data points.

values might also argue against a proton hopping mechanism. Moreover, the number of protons is very small in the case of present LDH-type materials and therefore its contribution to the dielectric loss is less probable.

The samples used for the dielectric measurements consist of pressed pellets. So the absolute values of the dielectric strength cannot be compared directly. Therefore Figure 10 compares the dielectric strengths normalized to the value measured at lowest temperature. The change in the temperature dependence of  $\Delta\epsilon$  for NiAlMo is much more pronounced than that of ZnAlMo. This can be discussed by taking into consideration the different thicknesses of the adsorbed water layers (see Table 2). For

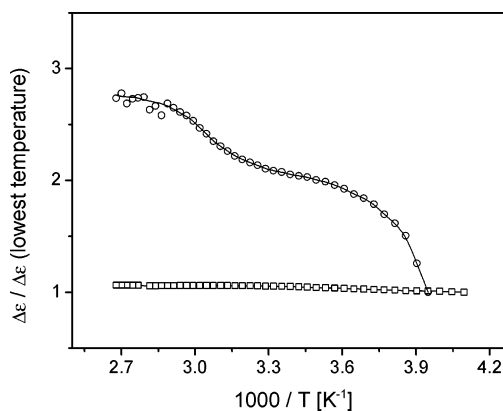


**Figure 10.** Reduced dielectric strength vs reciprocal temperature: (□) ZnAlMo and (○) NiAlMo. Lines are guides for the eyes.

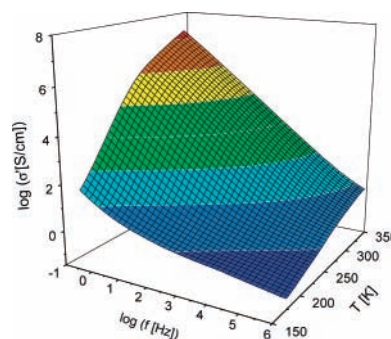


**Figure 11.** Real part of the complex conductivity  $\sigma'$  vs frequency and temperature for NaBIR in a 3D representation.

NiAlMo the water layer is one-third thicker than that for ZnAlMo. This means first that more water molecules contribute to the dielectric relaxation and so the absolute values of  $\Delta\epsilon$  are higher for NiAlMo than that for ZnAlMo (compare Figures 5B and 7B). Second, because the water layer is essentially thinner for ZnAlMo, for this system on average the molecules are more strongly bonded to the surface than for NiAlMo. If temperature is increased, the molecules become on average more mobile for NiAlMo than for ZnAlMo, which leads to a stronger temperature dependence of  $\Delta\epsilon$  of the former material.

(c) *NaBIR*. The conductivity of NaBIR is essentially higher than that of the two LDH materials. Therefore the real part of the complex conductivity instead of the dielectric loss is given in Figure 11 versus frequency and temperature. There might be two reasons for the essentially higher conductivity of NaBIR in comparison with the LDH materials. First, the sodium ion in the interlayer galleries is essentially smaller than the hepta-

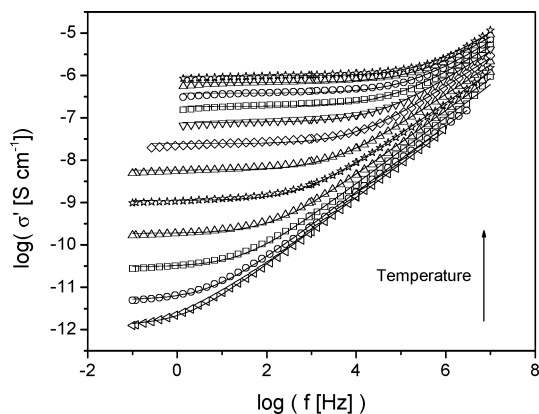


**Figure 12.** Real part of the complex conductivity vs frequency for different temperatures: (left-pointing triangles) 173.1, (○) 188.2, (□) 203.2, (△) 218.2, (☆) 233.2, (△) 248.2, (◇) 263.2, (▽) 278.2, (□) 293.1, (○) 308.1, (△) 323.1, and (☆) 338.1 K. Lines are fits according to eq 3.

molybdate anion in layered hydroxides and hence has a higher mobility than the latter one. In addition to the size, the heptamolybdate anions can be also bonded more tightly to the surfaces of the layers. This stronger interaction reduces the mobility of the heptamolybdate anions further. Conductivity is related to the number density of charges times their mobility. So this should lead to an essentially higher conductivity for NaBIR with regard to LDH materials even in the case that the number density of charges is comparable. This might be the most important fact. Second, the distance between the layers is smaller for NaBIR than for the LDH materials. This might have also an influence on the charge transport processes.

In comparison with Figure 4B, it is worth noting that no saddlelike shape of the spectra is observed in the raw data. Most likely the high conductivity of NaBIR hides the relaxation processes due to rotational fluctuations of water. Thus the dielectric loss spectrum of NaBIR does not show characteristic peaks due to relaxation processes.

To analyze the dielectric behavior of NaBIR in more detail, the real part of the complex conductivity is plotted versus frequency for different temperatures in Figure 12. As the first result the frequency and temperature dependence of the conductivity of NaBIR shows the well-known universal features of semiconducting disordered materials.<sup>39</sup> For low frequencies a plateau value is obtained for  $\sigma'$ , which can be extrapolated to the dc conductivity  $\sigma_0$  for  $f \rightarrow 0$ . At a critical frequency  $f_0$ , the dispersion of  $\sigma'$  sets in, resulting in a power law  $\sigma'(f) \sim f^s$  with  $0.5 \leq s \leq 1$ . For frequencies  $f < f_c$ , the temperature dependence of  $\sigma'(f)$  is much more pronounced than for  $f > f_c$ . For a review of the behavior of the complex conductivity of semiconducting disordered materials, see ref 40.

The conductivity is further analyzed in its frequency dependence by fitting the well-known Jonscher formula<sup>41</sup> to the data, which reads

$$\sigma'(f) = \sigma_0 + Af^s = \sigma_0[1 + (f/f_c)^s] \quad (6)$$

Equation 6 describes the data well (see Figure 12). In Figure 13 the dc conductivity is plotted versus  $f_c$ . A linear behavior is observed. This is a consequence of the Barton/Nakajima/Namikawa (BNN) relationship  $\sigma_0 \sim f_c$ .<sup>40</sup> The inset of Figure 13 gives the temperature dependence of dispersion parameter  $s$ .  $s$  decreases with increasing temperature. Both the BNN relationship and the temperature dependence are further universal features of the conductivity of semiconducting disordered

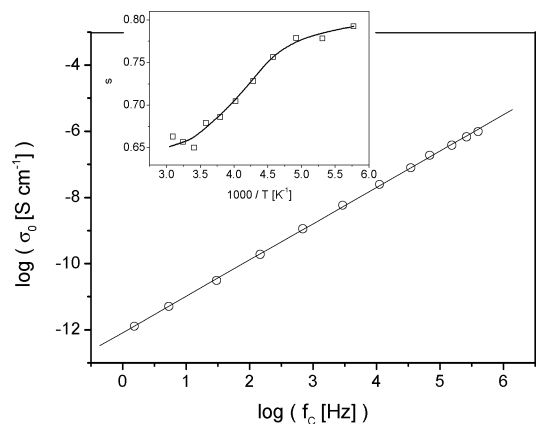


**Figure 13.** DC conductivity vs characteristic frequency for NaBIR. Not all the measured data are shown. The line is a linear regression to the data. (Inset) Dispersive index  $s$  vs reciprocal temperature.

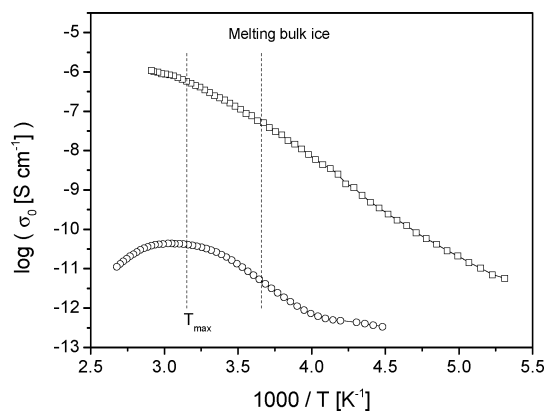


**Figure 14.** DC conductivity  $\sigma_0$  vs reciprocal temperature: (□) NaBIR and (○) NiAlMo. The temperature  $T_{\max}$  is taken from Figure 5A. Lines are guides for the eyes.

materials. In conclusion, the conductivity of NaBIR shows all the universal features for  $\sigma'(f, T)$  expected for semiconducting disordered materials.

In Figure 14 the dc conductivity of NaBIR is plotted versus reciprocal temperature. In addition, conductivity values of NiAlMo are also included. Because the relaxation process due to water molecules is observed in addition to the conductivity, the Jonscher formula cannot be used to estimate  $\sigma_0$  for NiAlMo. Thus the value at the lowest measured frequency is taken. As is already obvious from the raw data, the conductivity of NiAlMo is orders of magnitude lower than that of NaBIR. Its temperature dependence has a maximum at the same temperature where the relaxation rate  $f_p$  also has its maximum value.

The plateaulike structure of the temperature dependence of NaBIR conductivity is observed around  $T_{\max}$ . This might be regarded as a hint that in this layered material an unusual relaxation behavior takes place as well.

(d) *Nature of Defects.* One key parameter to model the temperature dependence of the relaxation times in the Ryabov model is the existence of defects. As was already discussed in refs 1 and 3, the question of the nature of the defects in these and related systems is still open. For water and ice, the nature of the orientation defects is complex, involving pairs of neighboring O...O atoms not bonded by hydrogen bonds or pairs of OH groups facing each other, OH...HO, depending on the microscopic environment of a considered defect. A jump of a defect to a new site occurs by a 120° rotation of a water molecule. In the case of water confined to porous systems, despite the suppression of forming tetrahedral hydrogen bonds,

there are even more possibilities to form defect sites, probably due to the presence of the framework of OH groups. In the case of the layered oxide materials, these bonds might involve the oxygen atoms of interlayer water or of the charge compensating ions. The interlayer composition has then to play an important role as well.

These parameters can be used to evaluate the “disorder” effects that appeared in the studied samples due to the additional OH groups or ions.

## Conclusions

The rotational fluctuations of water confined to layered oxide materials with brucite structure were investigated by broadband dielectric spectroscopy in a wide temperature range. Two different kinds of layered materials are considered, layered double hydroxide and birnessite. Both classes of layered materials differ essentially in their dielectric properties. For the LHD materials, besides conduction effects, a relaxation process was observed that is assigned to the reorientational fluctuations of water molecules adsorbed on the oxide surface or in the interlayer voids. A nonmonotonous temperature dependence of the relaxation rates of this relaxation process has been observed for layered double hydroxides NiAlMo or ZnAlMo. A quantitative description of this dependence was possible, based on a model assuming two competing processes: rotational fluctuation of water molecules and formation of additional defects. Reasonable values for the characteristic parameters were obtained. Furthermore, it is argued that the unusual temperature dependence of the observed relaxation process is not due to a substantial loss of water.

The activation energy of the rotational fluctuation, the pre-exponential factor, and the number of defects are higher whereas the value of the energy of defect formation is lower in the layered oxide materials than for water confined to nanoporous molecular sieves, porous glasses, or in bulk ice. By comparison of the different systems, it is found that the lower the energy of defect formation, the higher the number of defects. The prefactors increase with the activation energy as an expression of the compensation law, indicating the cooperative nature of the motional process.

For both NiAlMo and ZnAlMo the dielectric strength  $\Delta\epsilon$  of the observed relaxation process increases with increasing temperature. But the temperature dependence of  $\Delta\epsilon$  is much more pronounced for NiAlMo than for ZnAlMo. TGA experiments reveal that the water layer is essentially thicker for NiAlMo than for ZnAlMo. This result is used to explain the stronger temperature dependence of  $\Delta\epsilon$  observed for NiAlMo.

For birnessite the dielectric properties are dominated by a strong conductivity contribution, which is orders of magnitude higher than for the LDH materials. It is argued that the sodium ion in the interlayer galleries is highly mobile and so it is at the molecular origin of the high conductivity. The frequency and temperature dependence of the conductivity of NaBIR shows the features expected for the conductivity of semiconducting disordered materials. Especially the Barton/Nakajima/Namikawa relationship is obeyed. Comparison of the temperature dependence of the dc conductivity of NiAlMo with that of NaBIR gives some hints that also for NaBIR an unusual relaxation behavior takes place. This is further supported by a plateaulike structure of the temperature dependence of the conductivity observed around  $T_{\max}$ .

As a general conclusion, it is found that the behavior of water in layered oxide with brucite structure is similar to that observed for water in porous glasses and molecular sieves. Therefore it

is proven that it seems to be a quite fundamental phenomenon characteristic for water in confining geometries.

In the case of investigated LDH materials, the hydrogen bonds formed in the water might involve the oxygen atoms of the surface hydroxyl groups or of the charge-compensating ions. The interlayer composition has then to play an important role in the rotational dynamics of water as well. The characteristic parameters resulted from the applied model can be used to evaluate the “disorder” effects that appeared in the studied samples due to surface hydroxyl groups or interlayer ions.

**Acknowledgment.** Financial support by the Romanian Ministry of Education and Research (CERES Project 4-81) is gratefully acknowledged. L.F. and S.F. thank the German Academic Exchange Service for research fellowships and the Federal Institute of Materials Research and Testing (BAM) for permanent logistic support. Participation grants at the International Symposium “Catalytic processes on advanced micro- and mesoporous materials”, Nessebar, Bulgaria, and at the second CONCORDE conference held in Thessaloniki, Greece, are also highly appreciated. D.C., C.M., and V.R. acknowledge MEC financial support by Grant MAT2006-10800-C02-01. National Institute of Materials Physics (Romania), University of Bucharest (Romania), and Universidad de Salamanca (Spain) were partners in CA Type EU Project CONCORDE (2004–2006).

## References and Notes

- (1) Frunza, L.; Kosslick, H.; Pitsch, I.; Frunza, S.; Schönhals, A. *J. Phys. Chem. B* **2005**, *109*, 9154.
- (2) (a) Ryabov, Ya.; Gutina, A.; Arkhipov, V.; Feldman, Yu. *J. Phys. Chem. B* **2001**, *105*, 1845. (b) Ryabov, Y. E.; Puzenko, A.; Feldman, Yu. *Phys. Rev. B* **2004**, *69*, 014204.
- (3) Frunza, L.; Kosslick, H.; Frunza, S.; Schönhals, A. *J. Phys. Chem. B* **2002**, *106*, 9191.
- (4) Tilocca, A.; Selloni, A. *Langmuir* **2004**, *20*, 8379.
- (5) Henderson, M. A. *Surf. Sci. Rep.* **2002**, *46*, 1.
- (6) Dimeo, R. M.; Neumann, D. A.; Glanville, Y.; Minor, D. B. *Phys. Rev. B* **2002**, *66*, 104201.
- (7) (a) Allmann, R.; Lohse, H. H. *N. Jhb. Miner. Mh.* **1966**, *6*, 161. (b) Ingram, L.; Jepsen, H. P. *N. Jhb. Miner. Mh.* **1967**, *36*, 465. (c) Taylor, H. F. W. *Miner. Mag.* **1973**, *39*, 377. (d) Miyata, S. *Clays Clay Miner.* **1983**, *31*, 305. (e) Reichle, W. T. *CHEMTECH* **1986**, *16*, 58. (f) Cavani, F.; Trifirò, F.; Vaccari, A. *Catal. Today* **1991**, *11*, 173.
- (8) Rives, V., Ed. *Layered Double Hydroxides: Present and Future*; Nova Science Publishers: Hauppauge, NY, 2001; Chapt. 1.
- (9) Carriazo, D.; Domingo, C.; Martín, C.; Rives, V. *Inorg. Chem.* **2006**, *45*, 1243.
- (10) Carriazo, D.; Martín, C.; Rives, V.; Popescu, A.; Cojocar, B.; Mandache, I.; Parvulescu, V. I. *Microporous Mesoporous Mater.* **2006**, *95*, 39.
- (11) Julien, C.; Massot, M.; Baddour-Hadjean, R.; Franger, S.; Bach, S.; Pereira-Ramos, J. P. *Solid State Ionics* **2003**, *159*, 345.
- (12) Prieto, O.; Rives, V. *Bol. Soc. Esp. Ceram. Vid.* **2000**, *39*, 233.
- (13) Rives, V.; Prieto, O.; Del Arco, M.; Fetcu, A.; Parvulescu, V. I. In *Proceedings of the 14th International Zeolite Conference*; van Steen, E., et al., Eds.; DTT: Cape Town, South Africa, 2004; CD p 2639.
- (14) Prieto, O.; del Arco, M.; Rives, V. *Thermochim. Acta* **2003**, *41*, 95.
- (15) For example: Hunger, B.; Klepel, O.; Kirschhock, C.; Heuchel, M.; Toufar, H.; Fuess, H. *Langmuir* **1999**, *15*, 5937.
- (16) Schlosser, E.; Schönhals, A. *Colloid Polym. Sci.* **1989**, *267*, 963.
- (17) Schönhals, A.; Kremer, F. In *Broadband Dielectric Spectroscopy*; Kremer, F., Schönhals, A., Eds.; Springer-Verlag: Berlin and Heidelberg, Germany, 2003; (a) pp 59f; (b) p 81; (c) pp 1ff.
- (18) Frunza, S.; Kosslick, H.; Schönhals, A.; Frunza, L.; Enache, I.; Beica, T. *J. Non-Cryst. Solids* **2003**, *325*, 103.
- (19) (a) Drezdon, M. A. *Inorg. Chem.* **1988**, *27*, 4628. (b) Crespo, I.; Barriga, C.; Rives, V.; Ulibarri, M. A. *Solid State Ionics* **1997**, *101*, 729.
- (20) Vucelic, M.; Moggridge, G. D.; Jones, W. J. *Phys. Chem.* **1995**, *99*, 8328.
- (21) (a) Narita, E.; Kaviratna, P. D.; Pinnavaia, T. J. *Chem. Commun.* **1993**, 60. (b) Dimotakis, E. D.; Pinnavaia, T. J. *Inorg. Chem.* **1990**, *29*, 2393.
- (22) Hibino, T.; Tsunashima, A. *Chem. Mater.* **1997**, *9*, 2082.

- (23) Chen, R.; Zavalij, P.; Whittingham, M. S. *Chem. Mater.* **1996**, *8*, 1275.
- (24) Gailliot, A.-C.; Larson, B.; Drits, V. A. *Chem. Mater.* **2005**, *17*, 2959.
- (25) Rives, V. *Mater. Chem. Phys.* **2002**, *75*, 19.
- (26) Jaubertie, C.; Holgado, M. J.; San, Roman, M. S.; Rives, V. *Chem. Mater.* **2006**, *18*, 3114.
- (27) (a) Kalinichev, A. G.; Kirkpatrick, R. J.; Cygan, R. T. *Am. Mineral.* **2000**, *85*, 1046. (b) Wang, J.-W.; Kalinichev, A. G.; Kirkpatrick, R. J.; Hou, X.-Q. *Chem. Mater.* **2001**, *13*, 145. (c) Hou, X.-Q.; Kalinichev, A. G.; Kirkpatrick, R. J. *Chem. Mater.* **2002**, *14*, 2078.
- (28) Frunza, S.; Frunza, L.; Schönhals, A.; Zubowa, H.-L.; Kosslick, H.; Carius, H.-E.; Fricke, R. *Chem. Phys. Lett.* **1999**, *307*, 167.
- (29) Hench, L. L.; West, J. K. *Chem. Rev.* **1990**, *60*, 33 and references therein.
- (30) da Silva, A.; Donoso, P.; Aegerter, M. A. *J. Non-Cryst. Solids* **1992**, *145*, 168.
- (31) (a) Cramer, Ch.; Cramer, Th.; Arndt, M.; Kremer, F.; Naji, L.; Stannarius, R. *Mol. Cryst. Liq. Cryst.* **1997**, *303*, 209. (b) Aliev, F. M.; Sinha, G. *Mat. Res. Soc. Proc.* **1996**, *411*, 125.
- (32) Rozanski, S. A.; Stannarius, R.; Groothues, H.; Kremer, F. *Liq. Cryst.* **1996**, *20*, 59.
- (33) (a) Franke, M. E.; Simon, U. *Solid State Ionics* **1999**, *118*, 311. (b) Simon, U.; Franke, M. E. *Microporous Mesoporous Mater.* **2000**, *41*, 1.
- (34) Hwang, D. W.; Sinha, A. K.; Cheng, C. Y.; Yu, T. Y.; Hwang, L. P. *J. Phys. Chem. B* **2001**, *105*, 5713.
- (35) Chan, R. K.; Davidson, D. W.; Whalley, E. J. *Chem. Phys.* **1965**, *43*, 2376.
- (36) Kremer F.; Schönhals A. In *Broadband Dielectric Spectroscopy*; Kremer, F., Schönhals, A., Eds.; Springer-Verlag; Berlin, 2002; pp 99–129.
- (37) (a) Bergman, R.; Swenson, J. *Nature* **2000**, *403*, 283. (b) Swenson, J.; Bergman, R.; Longeville, S. *J. Chem. Phys.* **2001**, *115*, 11299. (c) Jansson, H.; Swenson, J. *Eur. Phys. J. E* **2003**, *12* (s01), 013.
- (38) (a) Dyre, J. C. *J. Phys. C: Solid State Phys.* **1986**, *19*, 5655. (b) Yeloljn, A.; Movaghar, B.; Brantz, H. M. *Phys. Rev. B* **1992**, *46*, 1244.
- (39) Kremer, F.; Rozanski, S. A. In *Broadband Dielectric Spectroscopy*; Kremer, F., Schönhals, A., Eds.; Springer-Verlag; Berlin, 2002; pp 475–494.
- (40) Dyre, J. C.; Schroder, T. B. *Rev. Mod. Phys.* **2000**, *72*, 873.
- (41) (a) Jonscher, A. K. *Nature* **1977**, *267*, 673. (b) Jonscher, A. K. *Phys. Thin Films* **1980**, *11*, 205. (c) Almond, D. P.; Duncan, G. K.; West, A. R. *Solid State Ionics* **1983**, *8*, 159.